Representing Sheared Convective Boundary Layer by Zeroth- and First-Order-Jump Mixed-Layer Models: Large-Eddy Simulation Verification

DAVID PINO

Applied Physics Department, Technical University of Catalonia, and Institute for Space Studies of Catalonia (IEEC/CSIC), Barcelona, Spain

JORDI VILÀ-GUERAU DE ARELLANO

Meteorology and Air Quality Section, Wageningen University, Wageningen, Netherlands

SI-WAN KIM*

National Center for Atmospheric Research,+ Boulder, Colorado

(Manuscript received 11 July 2005, in final form 14 February 2006)

ABSTRACT

Dry convective boundary layers characterized by a significant wind shear on the surface and at the inversion are studied by means of the mixed-layer theory. Two different representations of the entrainment zone, each of which has a different closure of the entrainment heat flux, are considered. The simpler of the two is based on a sharp discontinuity at the inversion (zeroth-order jump), whereas the second one prescribes a finite depth of the inversion zone (first-order jump). Large-eddy simulation data are used to provide the initial conditions for the mixed-layer models, and to verify their results. Two different atmospheric boundary layers with different stratification in the free atmosphere are analyzed. It is shown that, despite the simplicity of the zeroth-order-jump model, it provides similar results to the first-order-jump model and can reproduce the evolution of the mixed-layer variables obtained by the large-eddy simulations in sheared convective boundary layers. The mixed-layer model with both closures compares better with the large-eddy simulation results in the atmospheric boundary layer characterized by a moderate wind shear and a weak temperature inversion. These results can be used to represent the flux of momentum, heat, and other scalars at the entrainment zone in general circulation or chemistry transport models.

1. Introduction

The description of the heat flux at the interface between the atmospheric boundary layer and the free troposphere is still crudely represented in large atmospheric and chemistry models. In particular, the entrainment of warm and dry air is a crucial process in the growth of the convective boundary layer (CBL). This process depends closely on the different physical contributions to the turbulent kinetic energy (TKE) at the interface. In representing these fluxes at the entrainment zone in large-scale atmospheric models, it is advisable to include the most relevant processes but, in addition, to consider a simplified description of them.

Despite its simplicity, the mixed-layer, or slab, model (MXL), which assumes a homogeneous and instantaneous distribution of the state variables in the mixed layer below the inversion (Lilly 1968; Carson 1973; Tennekes 1973; Betts 1973, 1974; Mahrt and Lenschow 1976), retains the main characteristics of the CBL and accurately represents its growth.

In this study, two representations of the entrainment processes are used in the MXL. The main difference in the assumptions of these parameterizations is based on the definition of the entrainment zone depth δ (see Fig. 1). The most basic approach, proposed first

* Current affiliation: Aeronomy Laboratory, National Oceanic and Atmospheric Administration, Boulder, Colorado.

+ The National Center for Atmospheric Research is sponsored by the National Science Foundation.

Corresponding author address: David Pino, Applied Physics Department, Technical University of Catalonia, Avd. del Canal Olímpic s/n, 08860 Castelldefels, Spain.
E-mail: david@fa.upc.edu

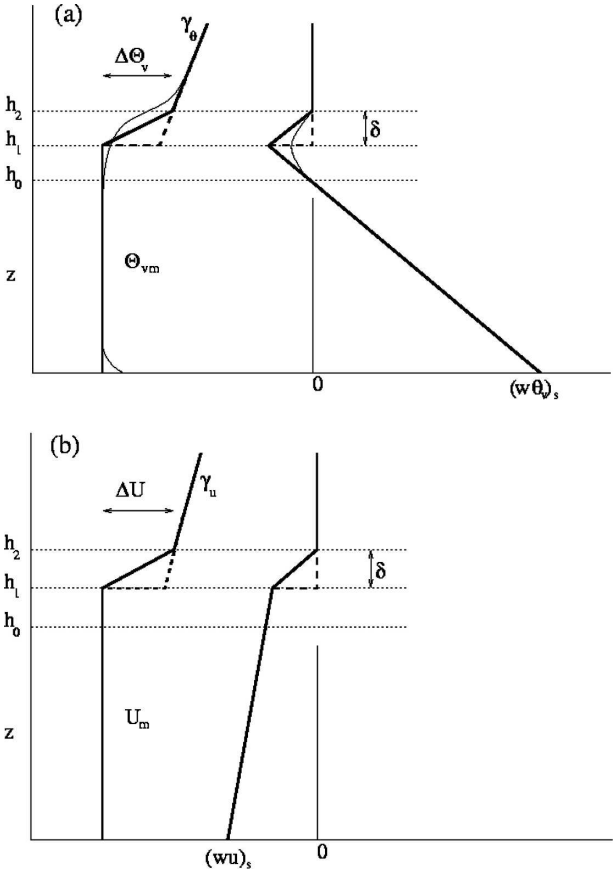

FIG. 1. Schematic representations of the vertical profiles of (a) the virtual potential temperature Θ_v and virtual potential temperature flux $\overline{w\theta_v}$ and (b) the mean wind in the x direction U_m and its momentum flux $\overline{wu}$, by means of a zeroth-order-jump (dashed) and a first-order-jump (solid) model. The thin lines in (a) represent an approximated real profile.

by Lilly (1968), represents the entrainment zone as a sharp discontinuous inversion ($\delta = 0$), namely, a zeroth-order-jump model (ZOJ). From the 1970s onward, and with different degrees of complexity, this approach has been widely applied to study the CBL over land (Tennekes 1973; Betts 1973; Carson 1973; Stull 1976b; Zeman and Tennekes 1977; Tennekes and Driedonks 1981; Driedonks and Tennekes 1984; Boers et al. 1984; Fedorovich 1995; Lilly 2002a; Pino et al. 2003), the stratocumulus-topped boundary layer (Pelly and Belcher 2001), the formation of a coastal internal boundary layer (Gryning and Batchvarova 1990; Källstrand and Smedman 1997; Flamant et al. 1999), the marine boundary layer (Flamant and Pelon 1996), and the impact of boundary layer dynamics on the carbon dioxide concentration or on the atmospheric chemistry in the CBL (de Arellano et al. 2004; Vinuesa and Vilà-Guerau de Arellano 2005).

The interface layer can also be described in a parametric form by a more realistic assumption. The entrainment region is assumed to have a finite thickness ($\delta \neq 0$), the so-called first-order-jump model (FOJ). An additional requirement in this description is the estimation of the inversion-layer thickness (Mahrt and Lenschow 1976; Deardorff et al. 1980; Garratt et al. 1982; Fairall 1984; Gryning and Batchvarova 1994; Kim et al. 2006, hereinafter KIM06).

In the MXL, regardless of the representation of the inversion layer ($\delta = 0$ or $\delta \neq 0$), the equations for heat, moisture, and momentum require an additional assumption to solve the closure problem (Stull 1988; Garratt 1992). Because of the key role played by the heat introduced across the inversion zone in the CBL development, the heat flux in the interface zone is usually prescribed to solve this closure problem. Therefore, it is assumed that the entrainment heat flux is a fraction of the surface heat flux, $\overline{w\theta_v}|_e = -\beta\overline{w\theta_v}|_s$. Previous research studies (Zeman and Tennekes 1977; Tennekes and Driedonks 1981; Driedonks 1982; Gryning and Batchvarova 1990; Flamant and Pelon 1996; Lilly 2002b; Pino et al. 2003; Sorbjan 2004) have directed their efforts toward developing a suitable parameterization of this ratio. These representations include, in addition to the loss of turbulent kinetic energy by the buoyancy process, the production of TKE by the presence of wind shear, and other contributions to the TKE budget. In conditions in which shear-generated turbulence is negligible, a constant value of $\beta = 0.2$ has provided satisfactory results (Stull 1976a). Water-tank experiments (Deardorff et al. 1980) and large-eddy simulations (LES) (Moeng and Sullivan 1994; van Zanten et al. 1999; Pino et al. 2003) corroborated this ratio. However, numerical simulations and observations have also shown that, depending on the wind shear, on thermal stratification in the free atmosphere, or on the inversion strength, β can vary between 0.1 and 0.4 (Betts 1973; Carson 1973; Rayment and Readings 1974; Cattle and Weston 1975; Flamant and Pelon 1996; Flamant et al. 1997; Betts et al. 1992; Angevine et al. 1998; Fedorovich et al. 2001, 2004a,b; Kim et al. 2003; Pino et al. 2003; de Arellano et al. 2004). It is important to note that the estimation based on observations usually involves much uncertainty.

To validate further the derived parameterizations in a CBL, observations (Mahrt and Lenschow 1976; Caughey and Palmer 1979; Artaz and André 1980; Dubosclard 1980; Garratt et al. 1982; Driedonks and Tennekes 1984; Fairall 1984; Culf 1992; Villani et al. 2005), and lately large-eddy simulations of the CBL (Lock and MacVean 1999; Lilly 2002b; Pino et al. 2003; Conzemius and Fedorovich 2004) under different conditions of

shear and of inversion strength have been commonly used.

By using LES data as a verification reference, we investigate the ability of a mixed-layer model, using two different approaches (ZOJ and FOJ) and closure assumptions for the TKE at the entrainment zone, to reproduce the main characteristics of the evolution of a well-developed CBL. Several CBL characterized by different conditions of shear on the surface and at the interface and by different inversion strengths are under study.

The two closure assumptions are obtained from the TKE budget by using scaling arguments. To our knowledge, this is the first time that zeroth- and first-order mixed-layer approaches incorporating parameterizations of β, which include the shear contribution at the interface, have been tested and compared with LES. Two recent works compared several parameterizations of the entrainment heat flux by using LES (Conzemius and Fedorovich 2004) or by means of the ZOJ mixed-layer model and observations (Villani et al. 2005). Here, three major new features have been considered in comparison with these previous studies. First, in our work the LES data are used only to provide the initial values of the MXL and not to provide the atmospheric variables during the whole CBL evolution as done by Conzemius and Fedorovich (2004). Second, through a comparison of the ZOJ and the FOJ approaches, the importance of assuming a finite interface in the inversion layer is studied. Third, the two parameterizations of the entrainment heat flux used here incorporate the contribution of the shear at the interface to the entrainment flux. This term, which was not considered in the parameterizations analyzed by Villani et al. (2005), plays a major role in TKE production at the inversion under conditions in which baroclinicity is significant (Fedorovich et al. 2001; Pino et al. 2003).

The paper is structured as follows. In section 2 the mixed-layer model and the parameterizations for the entrainment heat flux are presented. Section 3 describes the LES setup and the definition of the mixed-layer-model initial values. The results of the intercomparison are discussed in section 4. Conclusions and future perspectives are summarized in the final section.

2. Parametric expressions for the entrainment heat flux

The evolution of two different CBLs influenced by shear on the surface and in the inversion zone are studied by means of LES and two different slab-model approaches: a zeroth-order jump and a first-order jump. A brief description of the mixed-layer model and the closure assumptions is given below.

a. Mixed-layer model

In the atmospheric boundary layer, if horizontal homogeneity is assumed, the mean equations for the horizontally averaged values of the virtual potential temperature (Θ_v) and the two velocity components (U, V) read (Stull 1988; Garratt 1992) as

$$\frac{\partial \Theta_v}{\partial t} = -\frac{\overline{\partial w\theta_v}}{\partial z} - W\frac{\partial \Theta_v}{\partial z}, \tag{1}$$

$$\frac{\partial U}{\partial t} = f(V - V_g) - \frac{\partial \overline{wu}}{\partial z} - W\frac{\partial U}{\partial z}, \quad \text{and} \tag{2}$$

$$\frac{\partial V}{\partial t} = -f(U - U_g) - \frac{\partial \overline{wv}}{\partial z} - W\frac{\partial V}{\partial z}, \tag{3}$$

where f is the Coriolis parameter, w is the vertical velocity, capital letters represent horizontally averaged variables, and lowercase letters represent the fluctuating parts. The variables $U_g(z) = U_{gs} + \gamma_u z$ and $V_g(z) = V_{gs} + \gamma_v z$ are the geostrophic horizontal velocities, where U_{gs} and V_{gs} are the characteristic values of the two components of the geostrophic velocity in the mixed layer and γ_u and γ_v are the vertical gradients of these components in the free troposphere (Fedorovich 1995).

By integrating Eqs. (1)–(3) with respect to height z through the whole planetary boundary layer, the time evolution of the mean values of Θ_v, U, and V in the mixed layer is obtained (Garratt 1992). The upper limit of the integration depends on the physical assumptions for the turbulent fluxes in the entrainment zone. The two studied representations of the convective boundary layer in the MXL are presented schematically in Fig. 1. This figure shows the vertical profiles of the horizontally averaged virtual potential temperature and its flux (Fig. 1a) and the mean wind in the x direction and its momentum flux (Fig. 1b) according to the definitions applied in the ZOJ and FOJ models. In a first-order-jump model, Eqs. (1)–(3) are integrated from 0 to h_1, from h_1 to h_2, and from h_2 to $h_2 + \epsilon$, and the limit $\epsilon \to 0$ is taken after the integration. In a zeroth-order-jump model, in which the inversion layer is characterized by a sharp discontinuity, Eqs. (1)–(3) are integrated vertically from 0 to h_1 and from h_1 to $h_1 + \epsilon$ ($\epsilon \to 0$).

To perform the integration, three assumptions about the inversion layer and the free atmosphere aloft are made. First, the mean vertical velocity at h_1 (w_h) is assumed to be zero (Stull 1988), that is, mean vertical subsidence is neglected. The entrainment velocity is consequently defined as $w_e = \partial h_1/\partial t$. Second, though the structure of the inversion layer varies substantially in time, as observed by Rayment and Readings (1974), we follow here the same approach suggested by Betts

(1974) and also used by Mahrt and Lenschow (1976) and by van Zanten et al. (1999): to neglect in the heat balance equation in the inversion layer the term that accounts for the temporal variations of the inversion structure in the FOJ; that is, we assume $\partial\delta/\partial t = 0$ ($\delta = h_2 - h_1$). This assumption is supported by Sullivan et al. (1998), who show by analyzing LES results that the term, which includes $\partial\delta/\partial t$ in the heat balance equation at the interface, is negligibly small in comparison with the other terms (see section 7c and Fig. 22c of Sullivan et al. 1998). It is important to notice that this assumption does not imply that δ is constant with time; that is, $d\delta/dt \neq 0$. A diagnostic equation is consequently included to estimate the variation of δ. This expression of δ depends on several atmospheric variables: h_1, Θ_v, wind shear, and virtual potential temperature jump at the inversion. Note that these variables evolve with time during the development of the boundary layer. The third assumption is that the vertical gradients of the virtual potential temperature and horizontal velocities above the inversion are constant in time, $\partial\gamma_\theta/\partial t = \partial\gamma_u/\partial t = \partial\gamma_v/\partial t = 0$.

The resulting governing equations for the MXL, once the integration is performed using the Leibniz rule for the temporal term, read (Mahrt and Lenschow 1976) as

$$\frac{\partial\Theta_{vm}}{\partial t} = h_1^{-1}(\overline{w\theta_v}|_s - \overline{w\theta_v}|_{h_1}), \tag{4}$$

$$\Delta\Theta_v\frac{\partial h_1}{\partial t} = \delta\frac{\partial(\Theta_{vm} + 0.5\Delta\Theta_v)}{\partial t} - \overline{w\theta_v}|_{h_1}, \tag{5}$$

$$\frac{\partial\Delta\Theta_v}{\partial t} = \gamma_\theta\frac{\partial h_1}{\partial t} - \frac{\partial\Theta_{vm}}{\partial t}, \tag{6}$$

$$\frac{\partial U_m}{\partial t} = -f\Delta V + h_1^{-1}(\overline{wu}|_s - \overline{wu}|_{h_1}), \tag{7}$$

$$\Delta U\frac{\partial h_1}{\partial t} = \delta\frac{\partial(U_m + 0.5\Delta U)}{\partial t} - \overline{wu}|_{h_1} + 0.5f\delta\Delta V, \tag{8}$$

$$\frac{\partial\Delta U}{\partial t} = \gamma_u\frac{\partial h_1}{\partial t} - \frac{\partial U_m}{\partial t}, \tag{9}$$

$$\frac{\partial V_m}{\partial t} = f\Delta U + h_1^{-1}(\overline{wv}|_s - \overline{wv}|_{h_1}), \tag{10}$$

$$\Delta V\frac{\partial h_1}{\partial t} = \delta\frac{\partial(V_m + 0.5\Delta V)}{\partial t} - \overline{wv}|_{h_1} - 0.5f\delta\Delta U, \quad \text{and} \tag{11}$$

$$\frac{\partial\Delta V}{\partial t} = \gamma_v\frac{\partial h_1}{\partial t} - \frac{\partial V_m}{\partial t}, \tag{12}$$

where Θ_{vm}, U_m, and V_m are the slab values of the virtual potential temperature and of the horizontal velocities in the mixed layer; $\Delta\Theta_v$, $\Delta U = U_{gs} + \gamma_u h_1 - U_m$, and $\Delta V = V_{gs} + \gamma_v h_1 - V_m$, are the jumps of the virtual potential temperature and of the horizontal velocities at the inversion, and $\overline{w\theta_v}|_s$, $\overline{wu}|_s$, $\overline{wv}|_s$, $\overline{w\theta_v}|_{h_1}$, $\overline{wu}|_{h_1}$, and $\overline{wv}|_{h_1}$ are the heat and momentum fluxes on the surface and at h_1 respectively. Notice that the ZOJ model equations (Tennekes and Driedonks 1981) are retrieved by prescribing $\delta = 0$ in Eqs. (4)–(12). Equation (5) relates the amount of heat entrained into the boundary layer to the slab virtual potential temperature and the thickness of the entrainment zone.

Before proceeding, it is interesting to analyze in detail some of the simplifications and assumptions used in the literature to study the mixed-layer equations related to the momentum and heat flux at the entrainment zone [Eqs. (5), (8), and (11)]. When the inversion layer is negligible relative to the boundary layer depth, $\delta/h_1 \ll 1$, and by using Eq. (4), the entrainment virtual potential temperature flux becomes (Mahrt and Lenschow 1976)

$$\overline{w\theta_v}|_{h_1} = -\frac{\partial h_1}{\partial t}\Delta\Theta_v + \frac{\delta}{2}\frac{\partial\Delta\Theta_v}{\partial t}. \tag{13}$$

Equation (13) shows that the heat flux entrained in the mixed layer has two components in an FOJ approach. The second right-hand-side term shows the dependence of the entrainment flux on the evolution of the inversion jump and, in the studied cases, is approximately one-tenth of the magnitude of the first right-hand-side term because of the small variation of the virtual potential temperature jump during the boundary layer evolution. A similar analysis holds for the momentum fluxes at the interface. We obtain the following expressions:

$$\overline{wu}|_{h_1} = -\frac{\partial h_1}{\partial t}\Delta U + \frac{\delta}{2}\frac{\partial\Delta U}{\partial t} - \frac{\delta}{2}f\Delta V \quad \text{and} \tag{14}$$

$$\overline{wv}|_{h_1} = -\frac{\partial h_1}{\partial t}\Delta V + \frac{\delta}{2}\frac{\partial\Delta V}{\partial t} + \frac{\delta}{2}f\Delta U, \tag{15}$$

which, except for the last term in each expression that represents the Coriolis contribution, are similar to Eq. (13). From Eqs. (13)–(15), the entrainment fluxes for the ZOJ (Lilly 1968) are prescribed by setting $\delta = 0$ as follows:

$$\overline{w\theta_v}|_{h_1} = -\frac{\partial h_1}{\partial t}\Delta\Theta_v, \overline{wu}|_{h_1} = -\frac{\partial h_1}{\partial t}\Delta U, \quad \text{and}$$

$$\overline{wv}|_{h_1} = -\frac{\partial h_1}{\partial t}\Delta V, \tag{16}$$

which are exactly the same as Eqs. (5), (8), and (11) with $\delta = 0$.

Equations (4)–(12) have more unknown variables

than available equations. If γ_θ, γ_u, γ_v, and the surface fluxes are known, Eqs. (4)–(12) contain 11 unknowns: h_1, δ, Θ_{vm}, U_m, V_m, $\Delta\Theta_v$, ΔU, ΔV, and the heat and momentum fluxes at h_1. To close the equation set, the entrainment heat flux is usually assumed to be a function of the other mixed-layer variables. In addition, the inversion-layer thickness needs to be calculated in the case of FOJ (Mahrt and Lenschow 1976; Deardorff et al. 1980; KIM06). The diagnostic equation used to calculate δ was derived in KIM06. By using a parcel method, and taking into account the influence of the shear and temperature jump at the inversion, this equation reads

$$\delta = h_1(a\mathrm{Ri}^{-1} + b), \tag{17}$$

where $a = 1.12$ and $b = 0.08$ have been obtained by a least squares quadratic fit and Ri is a Richardson number defined as

$$\mathrm{Ri} = \frac{gh_1\Delta\Theta_v}{\Theta_{vm}w_\delta^2}, \tag{18}$$

with $w_\delta^2 = w_*^2 + 4u_*^2 + 0.1(\Delta U^2 + \Delta V^2)$, where u_* and w_* are the friction and convective velocities.

b. Parameterization of the heat flux at the interface

The most common assumption to represent the heat flux at the interface is to prescribe it as a constant fraction of the surface heat flux, $\beta = 0.2$, which holds in the CBL entirely dominated by convection (Stull 1976a; Garratt 1992). However, studies based on LES (Moeng and Sullivan 1994; Sullivan et al. 1998; Kim et al. 2003; Pino et al. 2003; Fedorovich et al. 2004b) and, to a certain extent, sodar (Dubosclard 1980), wind profiler (Angevine et al. 1998), and aircraft observations (Betts et al. 1992), combined with other meteorological observations, have shown that depending on the CBL characteristics, β can be larger than 0.2 and can vary in time. Therefore, several attempts to parameterize the entrainment flux ratio were proposed to reproduce these features.

Because the heat flux at the interface depends on the evolution and distribution of the TKE at this level, to obtain an expression of the entrainment flux from the TKE equation follows naturally. By analyzing the relative importance of the various physical mechanisms in the TKE equation, one obtains an expression of the entrainment flux as a function of the mixed-layer variables. Under horizontally homogeneous conditions and without subsidence, the TKE budget is

$$\frac{\partial\overline{e}}{\partial t} = -\left(\overline{wu}\frac{\partial U}{\partial z} + \overline{wv}\frac{\partial V}{\partial z}\right) + \frac{g}{\overline{\Theta_v}}\overline{w\theta_v} - \frac{\partial\overline{we}}{\partial z} - \frac{1}{\overline{\rho_0}}\frac{\partial\overline{wp}}{\partial z} - \epsilon, \tag{19}$$

where g is the gravity, p is the pressure, $\overline{\rho_0}$ is a reference density, $\overline{e} = 0.5\overline{(u^2 + v^2 + w^2)}$ is the time average of the TKE, and ϵ is the molecular dissipation of the TKE. The term on the left-hand side of Eq. (19) represents the tendency of TKE, and the terms on the right-hand side are, respectively, the shear production, the buoyancy production, the turbulent transport, the pressure transport, and the molecular dissipation term. By using scaling arguments, one can represent each contribution of Eq. (19) as a function of the characteristic scales in the CBL. Two main approaches have been followed with regard to the analysis and scaling of the different terms of the TKE equation. The first one applies the TKE equation directly in the inversion layer (local), and the second one integrates the TKE over the mixed layer (integral). The two approaches are equivalent, and the only differences lie in the values of the constants that appear in the final expression obtained for β [for a review of some of the entrainment flux ratio parameterizations, see Tennekes and Driedonks (1981), Conzemius and Fedorovich (2004), and Villani et al. (2005)].

For the ZOJ used here, the parameterization obtained using the local approach of the TKE budget reads (Pino et al. 2003)

$$\beta_{\mathrm{ZOJ}} = C_F\left[1 + \eta^3\left(\frac{u_*}{w_*}\right)^3\right]\frac{1}{1 + C_T/\mathrm{Ri}_t - C_M/\mathrm{Ri}_{\mathrm{GS}}}, \tag{20}$$

where $C_F = 0.2$, $\eta = 2$, $C_T = 5$, and $C_M = 0.7$, and Ri_t and $\mathrm{Ri}_{\mathrm{GS}}$ are two bulk Richardson numbers defined as

$$\mathrm{Ri}_t = \frac{gh_1}{\Theta_{vm}}\frac{\Delta\Theta_v}{\sigma_m^2} \quad \text{and} \quad \mathrm{Ri}_{\mathrm{GS}} = \frac{gh_1}{\Theta_{vm}}\frac{\Delta\Theta_v}{(\Delta V_e)^2}, \tag{21}$$

where $\sigma_m = (w_*^3 + \eta^3u_*^3)^{1/3}$ is a characteristic turbulent velocity and $(\Delta V_e)^2 = (\Delta U)^2 + (\Delta V)^2$ is the modulus of the velocity inversion jump. This parameterization includes, apart from the buoyancy (Tennekes and Driedonks 1981) and the transport-pressure contributions (Tennekes 1973), the time tendency of the TKE term (Zilitinkevich 1975, 1991) and the influence of shear on the entrainment heat flux evolution (Zeman and Tennekes 1977; Tennekes and Driedonks 1981; Driedonks 1982).

The contribution of the dissipation, which scales with the boundary layer depth, is implicitly considered in the scaling of the turbulent transport, pressure, and shear terms (Zeman and Tennekes 1977; Pino et al. 2003). However, under the presence of local production terms

at the interface (shear, gravity waves) or large Richardson numbers (Driedonks 1981), local dissipation of the TKE might scale with the depth of the interface. This contribution, named anomalous dissipation by some authors (Driedonks 1981), has to be explicitly included in the parameterization as a separate term, and its contribution was neglected in Eq. (20).

The FOJ used in our study parameterizes the entrainment flux ratio based on the TKE budget integration (KIM06). The expression reads

$$\beta_{\mathrm{FOJ}} = \left[1 - \frac{\Theta_{vm}(\Delta V_e)^2}{2g(\Delta\Theta_v - 0.5\gamma_\theta\delta)(h_1 + \delta)} A_3\right]^{-1} \left\{A_1 \frac{1}{1 + \delta/h_1} + + A_2\left(\frac{u_*}{w'_*}\right)^3 + A_3 \frac{\delta}{(4h_1 + 2\delta)}\left[\frac{u_*^2 \Delta V_e}{w'^3_*} + \frac{\Theta_{vm}(\Delta V_e)^2}{g(h_1 + \delta)(\Delta\Theta_v - 0.5\gamma_\theta\delta)}\right]\right\}, \tag{22}$$

where $w'^3_* = g\overline{w\theta_v}|_s(h_1 + \delta)/\Theta_{vm}$ and $A_1 = 0.2$, $A_2 = 0.26$, and $A_3 = 1.44$ are constants. The other symbols have the same meaning as in Eq. (20). Equation (22) slightly differs from to the one described by KIM06. Therein, the characteristic velocity scale at the inversion was defined as $\Delta\hat{U} = 0.5(|\Delta U| + |\Delta V|)$. In our research, by using the same $\Delta V_e = [(\Delta U)^2 + (\Delta V)^2]^{0.5}$ in both ZOJ and FOJ approaches, we prescribe the same velocity scaling at the inversion and the same initial condition for the modeling intercomparison. By so doing, we focus the discussion on the contributions of the different terms of the TKE equation on both approaches. In addition, we can retrieve ZOJ parameterization from FOJ by imposing $\delta = 0$. Last, it is important to notice that the results obtained by using the original velocity are only shown as a reference for different FOJ approaches.

The FOJ approach includes the buoyancy, the pressure, the shear, and the nonlocal dissipation contributions to the TKE (Zeman and Tennekes 1977; Driedonks 1982) but not the temporal change of the TKE, which can be important during the first stages of the CBL evolution and for very small inversion jumps (Tennekes 1973; Zilitinkevich 1975; Randall 1984). The way in which the dissipation contribution is included in the parameterization of the entrainment heat flux and the nature of its characteristic length scale are still open to debate. Here, the dissipation term is explicitly included in the FOJ by assuming that it is proportional to the flux and, similar to the ZOJ, its characteristic length scale coincides with the boundary layer depth (Zeman and Tennekes 1977; KIM06). By doing this, the inclusion of the dissipation effects reduce the contribution surface shear to the growth of the boundary layer depth.

The main difference between the β parameterization of the ZOJ and of the FOJ is the inclusion in the latter model of δ. In fact, if $\delta = 0$ is prescribed in Eq. (22), the entrainment flux ratio reads

$$\beta_{\mathrm{FOJ}}(\delta = 0) = A_1\left[1 + A'_2\left(\frac{u_*}{w_*}\right)^3\right]\frac{1}{1 - A'_3/\mathrm{Ri}_{\mathrm{GS}}}, \tag{23}$$

where $A'_2 = A_2/A_1 = 1.3$ and $A'_3 = A_3/2 = 0.72$. Therefore, when $\delta = 0$, Eq. (23) is similar to Eq. (20) but without taking into account the time tendency to the TKE. It is important to notice that $A_1 = C_F$; as a consequence, both parameterizations prescribe the same value of β for a pure convective boundary layer. Furthermore, $A'_3 \approx C_M$, which accounts for the shear and nonlocal dissipation effects. On the contrary, $A'_2 < \eta^3$ because the nonlocal additional dissipation contribution reduces the contribution of the surface wind shear to the TKE in the FOJ (KIM06).

3. Description of the numerical experiment

The evolution of two dry convective boundary layers characterized by shear on the surface and at the interface is modeled by the mixed-layer model discussed above. Particular emphasis is put on the impact of the assumption of sharp discontinuity (ZOJ) or finite discontinuity (FOJ) on the main CBL characteristics. We used the same external forcing for the mixed-layer model and for the LES. We simulated the atmospheric flows by means of LES to obtain the initial conditions for the mixed-layer model and to evaluate the MXL results.

a. Case description

The LES model is described by Cuijpers and Duynkerke (1993) and was lately modified by Cuijpers and Holtslag (1998). The domain is $10 \times 10 \times 2.032$

km^3 discretized by 256 × 256 × 64 points in each direction. We considered two different sheared CBLs by prescribing a constant-in-time surface virtual potential temperature flux equal to 0.1 K m s^{-1} and shear forcing (constant geostrophic wind of $U_g = 20$ m s^{-1} and $V_g = 0$ m s^{-1} in the whole domain), but different thermal stratification in the free atmosphere above the mixed layer: 1) case W (weak) has a temperature lapse rate $\gamma_{\theta(w)} = 0.003$ K m^{-1}, which produces a CBL with a weak capping inversion, and 2) case S (strong) has a temperature lapse rate $\gamma_{\theta(s)} = 0.006$ K m^{-1}, which results in a CBL with a strong capping inversion. For each case, the prescribed initial virtual potential temperature changes vertically from its surface value (300 K) at a constant rate of $\gamma_{\theta(w)}$ and $\gamma_{\theta(s)}$, respectively.

In the two cases, the initial mean wind is $U = 20$ m s^{-1} and $V = 0$ m s^{-1}, constant with height for the whole domain. The roughness length z_0 is 0.01 m, and the geographic latitude is $\phi = 40°$ ($f = 10^{-4}$ s^{-1}). The effects of humidity were not considered in the simulations. Turbulence statistics were calculated every 200 s. After approximately 1 h of simulation, the simulated flows approximately present a steady-state behavior; that is, the TKE does not change significantly with time. The average values, between 1 and 4 h, of the friction and convection velocities, respectively, are 0.73 and 1.47 m s^{-1} for case W and 0.70 and 1.33 m s^{-1} for case S.

To test the MXL, the evolution of the convective boundary layer was simulated with the mixed-layer model using the ZOJ and FOJ approaches and was compared with the LES results over a period of 10 000 s.

b. Initial conditions of the mixed-layer model

Once the simulated convective boundary layer was well formed, the LES results were used to provide the initial conditions in the ZOJ and the FOJ. Because of the different initial thermal stratification, the formation of a well-developed mixed layer can occur at different times, depending on the simulated case. Figure 2 shows the virtual potential temperature (Fig. 2a) and virtual potential temperature flux (Fig. 2b) vertical profiles obtained by the LES after 5000 s for case W and 8000 s for case S. In both cases, the vertical profiles of the mean and flux variables followed the characteristics of a well-developed CBL. Therefore, we initialized the MXL with the LES values at the above-mentioned times. As explained in section 2a, to solve Eqs. (4)–(12), the initial values of h_1, Θ_{vm}, U_m, V_m, $\Delta\Theta_v$, ΔU, ΔV, $\overline{w\theta_{v|s}}$, $\overline{wu}|_s$, and $\overline{wv}|_s$ have to be provided. Furthermore, in the case of the FOJ, the initial inversion-layer thickness must also be specified. Because of the different characterization of the inversion layer in the ZOJ and the FOJ approaches, the definition of the inversion jump values extracted from the LES differ between the ZOJ and FOJ. These jump values are used to initialize and evaluate the ZOJ and the FOJ. In the following sections, we give an exact description of the estimation of each variable (see also Fig. 1).

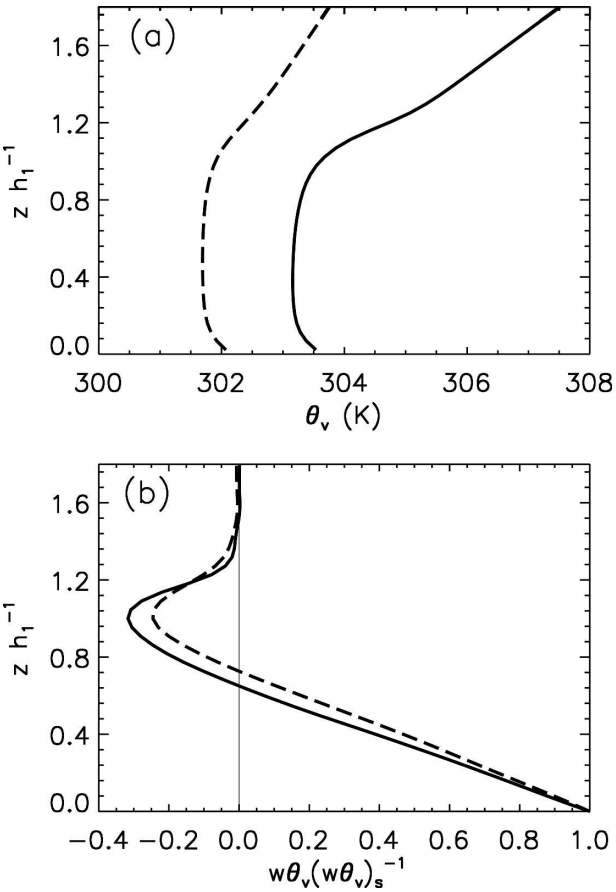

FIG. 2. Vertical profile of (a) the virtual potential temperature and (b) the virtual potential temperature flux, obtained by LES after 5000 s for case W (dashed) and after 8000 s for case S (solid).

1) BOUNDARY LAYER DEPTH

Boundary layer depth h_1 is defined as the height of the minimum virtual potential temperature flux. Some authors have used the height of the maximum virtual potential temperature gradient as the definition for the CBL depth (Sullivan et al. 1998; Lilly 2002a), and it was used by the authors in previous works (Fedorovich et al. 2004b). This definition is usually preferred because of its stability and, as will be shown later, provides higher values of the CBL depth than the one used here. However, we have defined the boundary layer depth as the minimum of the virtual potential temperature flux to keep consistency with the mixed-layer theory assumptions (Fedorovich et al. 2004a).

2) INVERSION-LAYER THICKNESS

Inversion-layer thickness is defined as $\delta = h_2 - h_1$. Here h_2 is not the height above h_1 at which the virtual potential temperature flux becomes zero but rather is that at which it is larger than 10% of its minimum value. This definition was used because at some specific times the virtual potential temperature flux becomes positive at unrealistic high values of z, especially for case W. However, by using this criterion, h_2 is below the height at which the virtual potential temperature flux becomes zero. Therefore, the $\delta = h_2 - h_1$ obtained by using this definition is slightly underestimated.

3) MEAN VALUES IN THE MIXED LAYER

The mean values in the mixed layer are defined as $\Theta_{vm} = \Theta_v(z = h_0/2)$, $U_m = U(z = h_0/2)$, and $V_m = V(z = h_0/2)$, where h_0 is the height below h_1 at which the virtual potential temperature flux becomes zero (lower crossing).

4) TEMPERATURE JUMP AT THE INVERSION

For this variable, because of the different physical assumptions of the entrainment zone in the ZOJ and the FOJ, two different definitions were used to initialize and compare the MXL results: $\Delta\Theta_{v(\mathrm{FOJ})} = \Theta_v(z = h_2) - \Theta_{vm}$ (KIM06) and $\Delta\Theta_{v(\mathrm{ZOJ})} = \Theta_v(z = h_2) - \gamma_\theta(h_2 - h_1) - \Theta_{vm}$ (Fedorovich et al. 2004a).

5) VELOCITY JUMPS AT THE INVERSION

To maintain consistency, these variables are defined in the same way as the temperature inversion jump for ZOJ and FOJ: $\Delta U_{(\mathrm{FOJ})} = U(z = h_2) - U_m$ and $\Delta U_{(\mathrm{ZOJ})} = U(z = h_2) - \gamma_u(h_2 - h_1) - U_m$, where $U(z = h_2) = U_g = 20\ \mathrm{m\ s^{-1}}$ and $V(z = h_2) = V_g = 0\ \mathrm{m\ s^{-1}}$. In the cases under study, $\gamma_u = \gamma_v = 0\ \mathrm{s^{-1}}$, and, therefore, $\Delta U_{\mathrm{ZOJ}} = \Delta U_{\mathrm{FOJ}}$. Similar definitions are used for ΔV.

6) SURFACE MOMENTUM FLUXES

The surface momentum fluxes are defined as $\overline{wu}|_s = \overline{wu}(z = 0)$ and $\overline{wv}|_s = \overline{wv}(z = 0)$. The evolution of the surface momentum fluxes for the MXL during 10 000 s is prescribed based on LES results. Cases W and S both show surface momentum fluxes that approximately have a linear evolution with time once the CBL is well developed. The particular expressions of the surface momentum fluxes have been obtained by performing a polynomial fit to the LES results for both cases. The expressions for the variation with time of the LES-derived surface momentum fluxes are not shown here.

Table 1 summarizes the prescribed initial values of h_1, δ, Θ_{vm}, $\Delta\Theta_v$, U_m, ΔU, V_m, ΔV, and u_* for the ZOJ and the FOJ in the weak-inversion and strong-inversion cases.

TABLE 1. Initial values for the mixed-layer model simulations of the atmospheric variables obtained from the LES results. The definition of each variable is explained in the text.

	Case W	Case S
h_1 (m)	750	704
δ (m)	250	190
Θ_{vm} (K)	301.75	303.16
$\Delta\Theta_{v(\mathrm{ZOJ})}$ (K)	0.45	1.04
$\Delta\Theta_{v(\mathrm{FOJ})}$ (K)	1.20	2.16
U_m (m s^{-1})	16.50	14.93
ΔU (m s^{-1})	3.50	5.07
V_m (m s^{-1})	0.83	1.85
ΔV (m s^{-1})	−0.83	−1.85
u_* (m s^{-1})	0.742	0.695

4. Results

We focus on the evolution of the boundary layer depth h_1, the entrainment velocity w_e, the virtual potential temperature and the wind mixed-layer values (Θ_{vm}, U_m, V_m), and the jumps at the inversion of these variables ($\Delta\Theta_v$, ΔU, ΔV). Furthermore, to make a specific analysis of the parameterizations of the entrainment flux ratio included in the MXL, two different variables are included in the comparison: the entrainment flux ratio β and the ratio between areas of positive and negative virtual potential temperature flux.

a. Boundary layer depth and entrainment velocity evolution

Figure 3 shows the time evolution of the boundary layer depth and the entrainment velocity simulated with the ZOJ, the FOJ, and the LES for the weak-inversion case. Figure 4 shows the evolution of the same variables for the strong-inversion case. For the LES, a least squares quadratic fit of the results of the height of the minimum virtual potential temperature flux and of the height of the maximum virtual potential temperature gradient (h_θ) is made to avoid the scatter of h_1, which particularly influences the calculation of the entrainment velocity. As the results show, and similar to Sullivan et al. (1998), for both inversion cases h_θ is always higher than h_1.

To study the effect of the other contributions of the TKE equation, in particular the shear production, on the ZOJ results, we performed an additional run assuming a constant value $\beta = 0.2$ in the ZOJ scheme. As shown in Figs. 3a and 4a, in this latter case the bound-

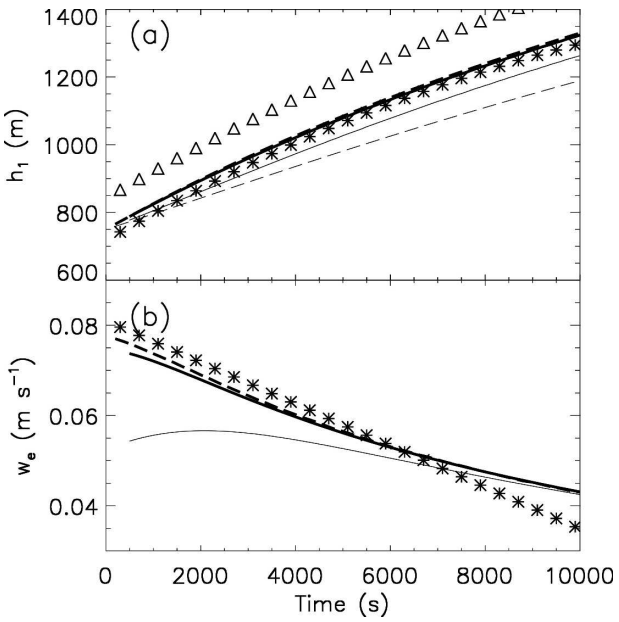

FIG. 3. Time evolution of (a) the boundary layer depth and (b) the entrainment velocity simulated by means of the LES (asterisks), the ZOJ (thick dashed line), and the FOJ (thick solid line) for the weak-inversion case. In (a) the thin dashed line represents the boundary layer depth time evolution simulated by the ZOJ prescribing $\beta = 0.2$ and the thin solid line represents the boundary layer depth time evolution obtained if the original velocity scale is used in the FOJ [also included in (b)]. In this figure, the triangles show the LES boundary layer depth calculated by means of the height of the maximum virtual potential temperature gradient.

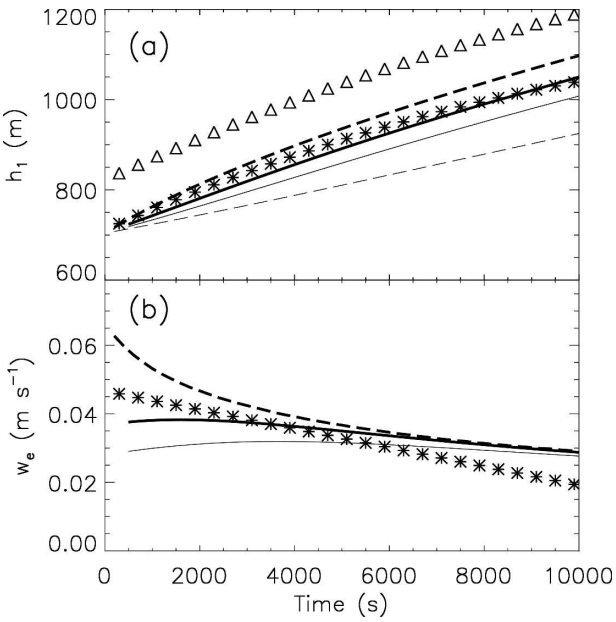

FIG. 4. Same as Fig. 3, but for the strong-inversion case.

ary layer depth is clearly underestimated over the whole period of integration by 9% for case W and by 14% for case S. Therefore, for the cases under study it is necessary to consider at least the shear (productive) contribution to the TKE, which increases the value of the entrainment heat flux, to simulate correctly the time evolution of the boundary layer depth by means of a ZOJ.

To show the influence of the definition of the velocity scale at the inversion (KIM06), we have also included at Figs. 3 and 4 the mixed-layer depth obtained by the FOJ if the original velocity scale at the inversion ($\Delta\hat{U}$) is prescribed. In the S and W cases, the FOJ parameterization that uses $\Delta\hat{U}$ underestimates LES results.

For the comparison between the MXL representations, Figs. 3a shows that both MXL approaches satisfactorily reproduce the values of the boundary layer depth calculated by the LES for case W. If the strong-inversion case is considered (Fig. 4a), the ZOJ tends to overestimate slightly, whereas the FOJ underestimates the boundary layer depth obtained by means of the LES. It is important to notice that this is a surprising result because one would expect that, at least for the W case, in which the inversion depth is important, the FOJ approach would have produced closer results to LES than would have the ZOJ approach.

The entrainment velocity is shown in Figs. 3b and 4b. The two MXL approaches approximately follow the evolution of the entrainment velocity obtained by the LES for both CBLs. As shown, the FOJ parameterization that uses $\Delta\hat{U}$ leads to lower values relative to LES results. To explain the differences that appear between both MXL, the calculation of the entrainment velocity by the models used in this study is explicitly shown. For the LES, the entrainment velocity is estimated by calculating the time derivative of the least squares fit of the height of the minimum virtual potential temperature flux:

$$w_{e(\mathrm{LES})} = \left.\frac{\partial h_1}{\partial t}\right|_{(\mathrm{LES})}. \tag{24}$$

In the ZOJ, the entrainment velocity is calculated as follows:

$$w_{e(\mathrm{ZOJ})} = \left.\frac{\partial h_1}{\partial t}\right|_{(\mathrm{ZOJ})} = -\frac{\beta_{\mathrm{ZOJ}}}{\Delta\Theta_{v(\mathrm{ZOJ})}}\,\overline{w\theta}_{v|s}, \tag{25}$$

whereas the FOJ calculates the entrainment velocity as (KIM06)

$$w_{e(\mathrm{FOJ})} = \left.\frac{\partial h_1}{\partial t}\right|_{(\mathrm{FOJ})} = \frac{\delta - (2h_1 + \delta)\beta_{\mathrm{FOJ}}}{h_1[2\Delta\Theta_{v(\mathrm{FOJ})} - \gamma_\theta\delta]}\,\overline{w\theta}_{v|s}, \tag{26}$$

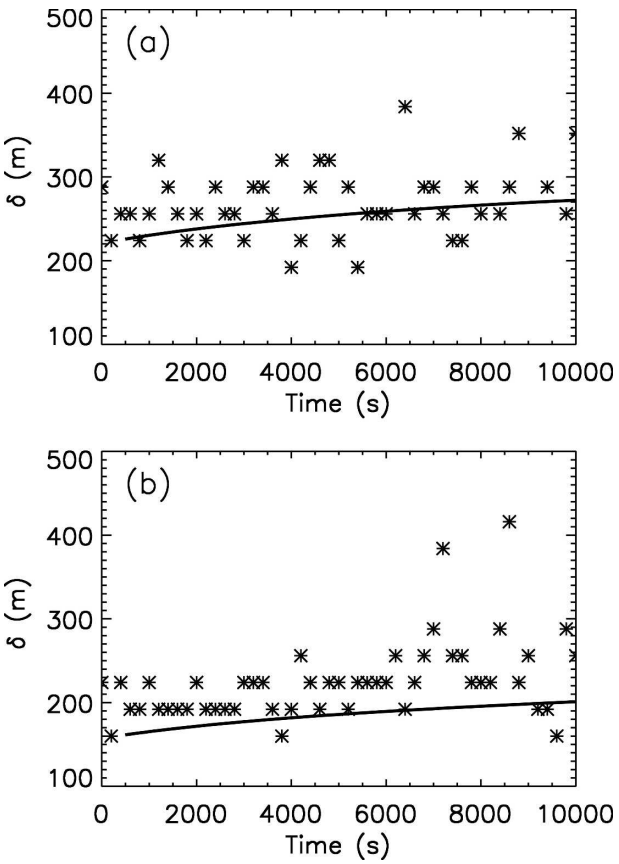

FIG. 5. Time evolution of the inversion-layer depth obtained for cases (a) W and (b) S by means of the LES (asterisks) and the FOJ (solid line).

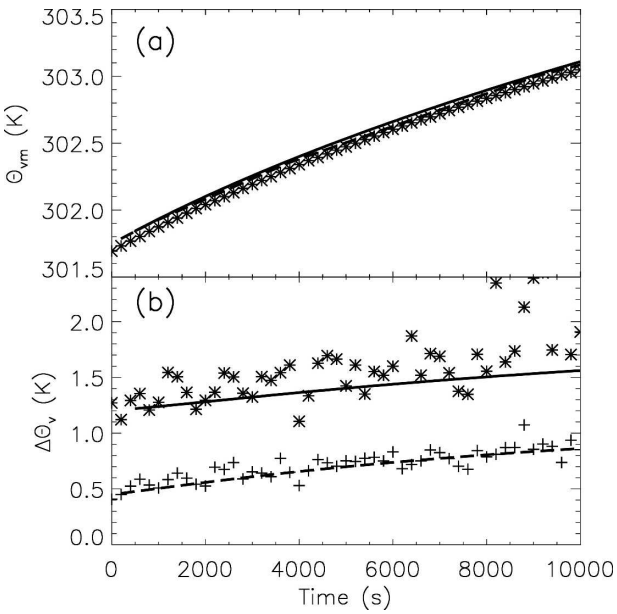

FIG. 6. Time evolution of (a) the mixed-layer virtual potential temperature and (b) the temperature jump at the inversion calculated by means of the LES (symbols), the ZOJ (dashed line), and the FOJ (solid line) for the weak-inversion case. Because of the different definition used for $\Delta\Theta_v$ extracted from the LES to compare with the ZOJ or the FOJ results, in (b) crosses are used to compare with the ZOJ and asterisks are used to compare with the FOJ.

where $\overline{w\theta}_{v|s} = 0.1$ K m s^{-1}. As expected, if $\delta = 0$, then $\Delta\Theta_{v(\mathrm{FOJ})} = \Delta\Theta_{v(\mathrm{ZOJ})}$, and Eq. (26) reduces to Eq. (25).

As occurred for the boundary layer height, both MXL approaches better reproduce the entrainment velocity obtained by means of LES for case W than for case S. By analyzing the expressions in Eqs. (25) and (26), one can conclude that the discrepancy between the LES and the MXL entrainment velocity occurs because the MXL does not correctly simulate (a) the temperature inversion jump or (b) the entrainment flux ratio or, (c) in the case of the FOJ, the inversion layer thickness obtained by the LES. To discriminate between the above-mentioned reasons, Fig. 5 shows the time evolution of the inversion-layer thickness calculated by the FOJ approach and the LES for the two inversion cases. As expected, the depth of the entrainment zone increases with the decreasing temperature inversion strength. It is important to notice here the scatter of the LES results for δ resulting from the variability in the calculation of h_2. Figure 5 shows that the FOJ reproduces the simulated evolution by means of LES of the inversion-layer depth satisfactorily for the two cases, with a slight underestimation for case S. Therefore, the overestimation of the entrainment velocity by FOJ is not caused because of a miscalculation of δ.

In section 4b, it is shown that the temperature jump evolution calculated by the MXL agrees satisfactorily with the LES results. Therefore, the discrepancy shown in Figs. 3b and 4b is the only clue to the overestimation of the entrainment heat flux by both MXL parameterizations (see section 4d for further discussion).

b. Mean virtual potential temperature and temperature inversion jump

The time evolution of the mean virtual potential temperature in the mixed layer and the temperature inversion jump for cases W and S are shown in Figs. 6 and 7, respectively. The MXL, with the parameterizations given in Eqs. (20) and (22), satisfactorily reproduces, with only a slight overestimation, the mean virtual potential temperature evolution obtained with the LES for both case W and case S. For the intercomparison of the temperature inversion jump (Figs. 6b and 7b), the ZOJ better reproduces the LES results than does the FOJ for the two inversion cases. As observed, the FOJ,

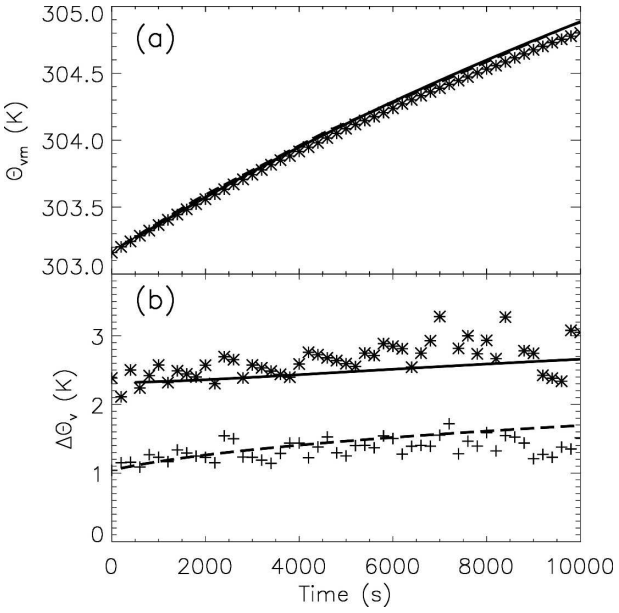

FIG. 7. Same as Fig. 6, but for the strong-inversion case.

in general, underestimates the temperature inversion jump obtained by the LES.

c. Mean wind and velocity inversion jump

Figures 8 and 9 show for the weak-inversion and strong-inversion cases, respectively, the mean wind in the mixed layer and the velocity jump at the inversion for the two components of the horizontal velocity. In comparison with the LES results, the wind evolution agrees better for case W than for case S. This fact can be explained by considering that in case S the local effects (shear and dissipation) at the inversion, not considered in the parameterizations of the entrainment fluxes, are potentially more important than in case W. For case W (Fig. 8), the ZOJ agrees better with the LES results than does the FOJ for both components of the mean horizontal velocity and inversion jumps. The good agreement for U_m is particularly noteworthy. For case S (Fig. 9), the MXL, both ZOJ and FOJ, do not model well the evolution of the wind characteristics. This is particularly evident for U_m (ΔU), which is overestimated (underestimated) by both MXL approaches. The V component is much better simulated by the MXL, especially by the ZOJ. For this case, as shown in Fig. 4b, MXL does not correctly fit the entrainment velocity calculated by means of the LES. Therefore, by taking into account Eq. (16), one can conclude that the entrainment momentum fluxes are also overestimated and, as a consequence, the mean velocities in the boundary layer are not correctly reproduced by MXL.

d. Entrainment flux ratio

One of the objectives of the study was to test the proposed parameterizations of the entrainment flux ratio implemented in the MXL. The parameterization proposed by Pino et al. (2003) has been previously compared with similar entrainment parameterizations (Zeman and Tennekes 1977; Tennekes and Driedonks 1981; Boers et al. 1984) for different sheared convective boundary layers by Conzemius and Fedorovich (2004). However, in that study the LES values were used as input variables of the considered parameterizations during the whole CBL evolution.

Figure 10 shows the β ratio calculated by means of Eq. (20) included in the ZOJ, by means of Eq. (22) included in the FOJ, and obtained from the LES results by calculating $\beta_{\mathrm{LES}} = -\overline{w\theta_v}|_{h_1}(\overline{w\theta_v}|_s)^{-1}$ for the two inversion cases. We have also included β obtained by using $\Delta\hat{U}$ as a reference. For this approach, LES results are correctly fitted. However, as mentioned previously, these lower β values yield an underestimation of the boundary layer depth and entrainment velocity evolution. It is important to notice that because the same constant surface flux is prescribed for all the models, Fig. 10 only represents the evolution of the virtual potential temperature flux at the entrainment zone. As was already pointed out (Pino et al. 2003; Conzemius and Fedorovich 2004), in the sheared convective boundary layer, β becomes larger with the increasing temperature inversion strength, or with the wind shear on the surface, or at the inversion. Therefore, the lowest β values are obtained for case W.

As shown, both parameterizations included in the MXL overestimate β when compared with the LES results. However, some differences can be observed between the parameterizations of β included in the MXL. For case W, β_{ZOJ} gives better results than β_{FOJ}, especially at the beginning of the simulation when the contribution of the temporal term of the TKE, considered only on the ZOJ description, is relevant.

By contrast, the parameterization included in the FOJ gives better results than those in the ZOJ for case S. In this case, the shear effects are an important contribution to the TKE at the inversion. Furthermore, because of the larger strength of the inversion in comparison with case W, the local dissipation effects might not be negligible. Conzemius and Fedorovich (2004) came up with a similar conclusion. They showed that a zeroth-order approach gives worse results than a first-order approach in the case of strong wind shear. This high overestimation of the entrainment heat flux by the ZOJ consequently has a direct influence on the calculation of w_e.

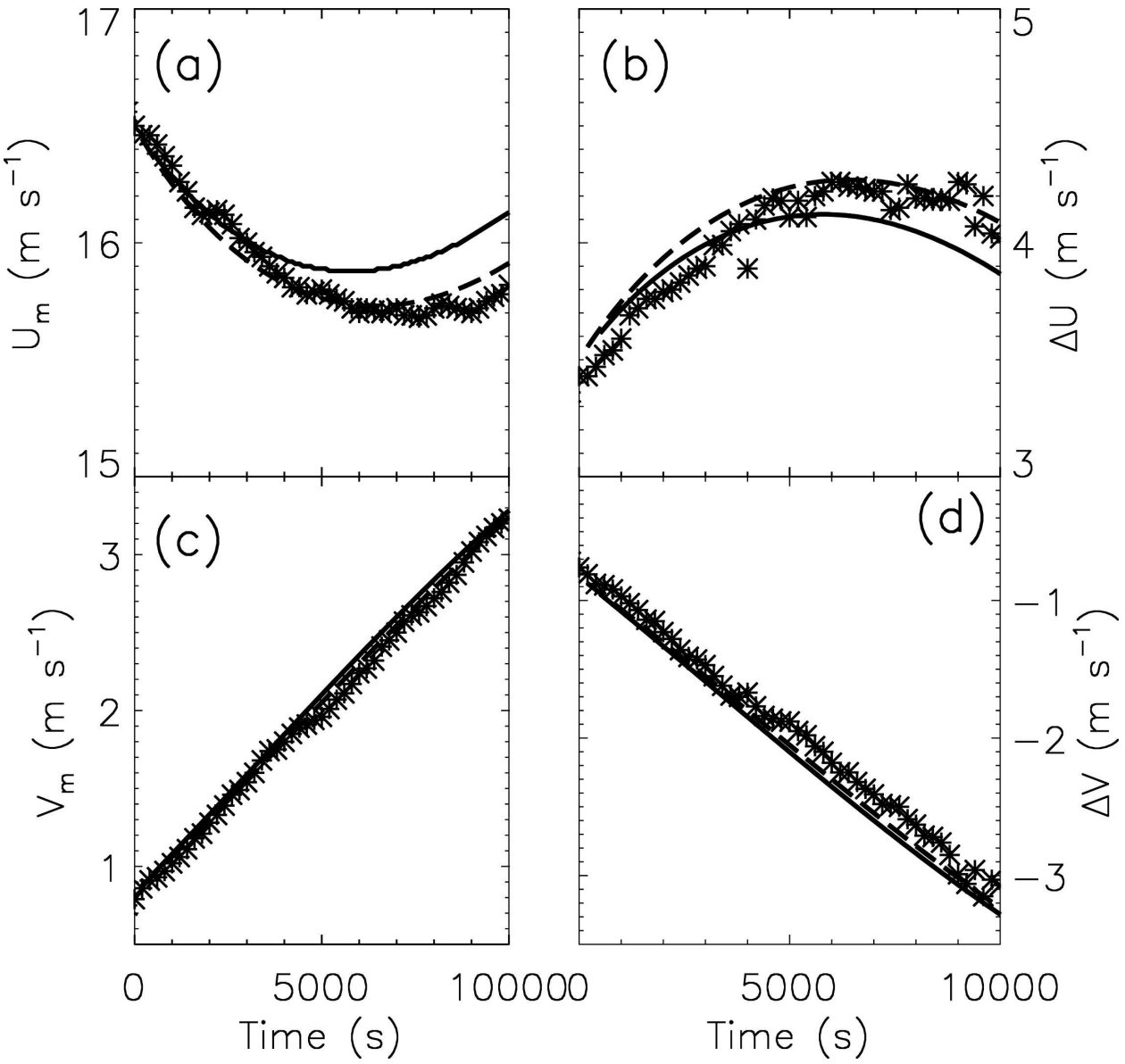

FIG. 8. Time evolution of the two components of (left) the mean wind and (right) their inversion jumps: (top) U and (bottom) V calculated by means of the LES (asterisks), the ZOJ (dashed line), and the FOJ (solid line) for the weak-inversion case.

Another important point in the discussion of the comparison of the entrainment fluxes between LES and MXL and two of the assumptions used to derive (20) and (22) are the possible reasons for the overestimation: (a) the MXL, which explicitly assumes that the virtual potential temperature flux is a linear profile up to h_1, always results in higher entrainment heat flux values than those obtained from the equivalent simulated LES profile (by analyzing the LES results, one can conclude that, in the studied cases, this approximation produces values of the virtual potential temperature flux at the inversion that are 1.5 times the LES value); (b) as Lilly (2002a) pointed out, LES entrainment fluxes are smoothed because of the horizontal average of the large-scale fluctuations at the mixed-layer top and therefore LES results always produce smaller results of the minimum virtual potential temperature flux when compared with the mixed-layer model; and (c) this effect may be further enhanced by the mathematical form of Eqs. (20) and (22), which include the elevated shear effect with a negative sign in the denominator. By using physical and scaling arguments, this contribution naturally appears in this form if the derivations of the parameterization from the TKE

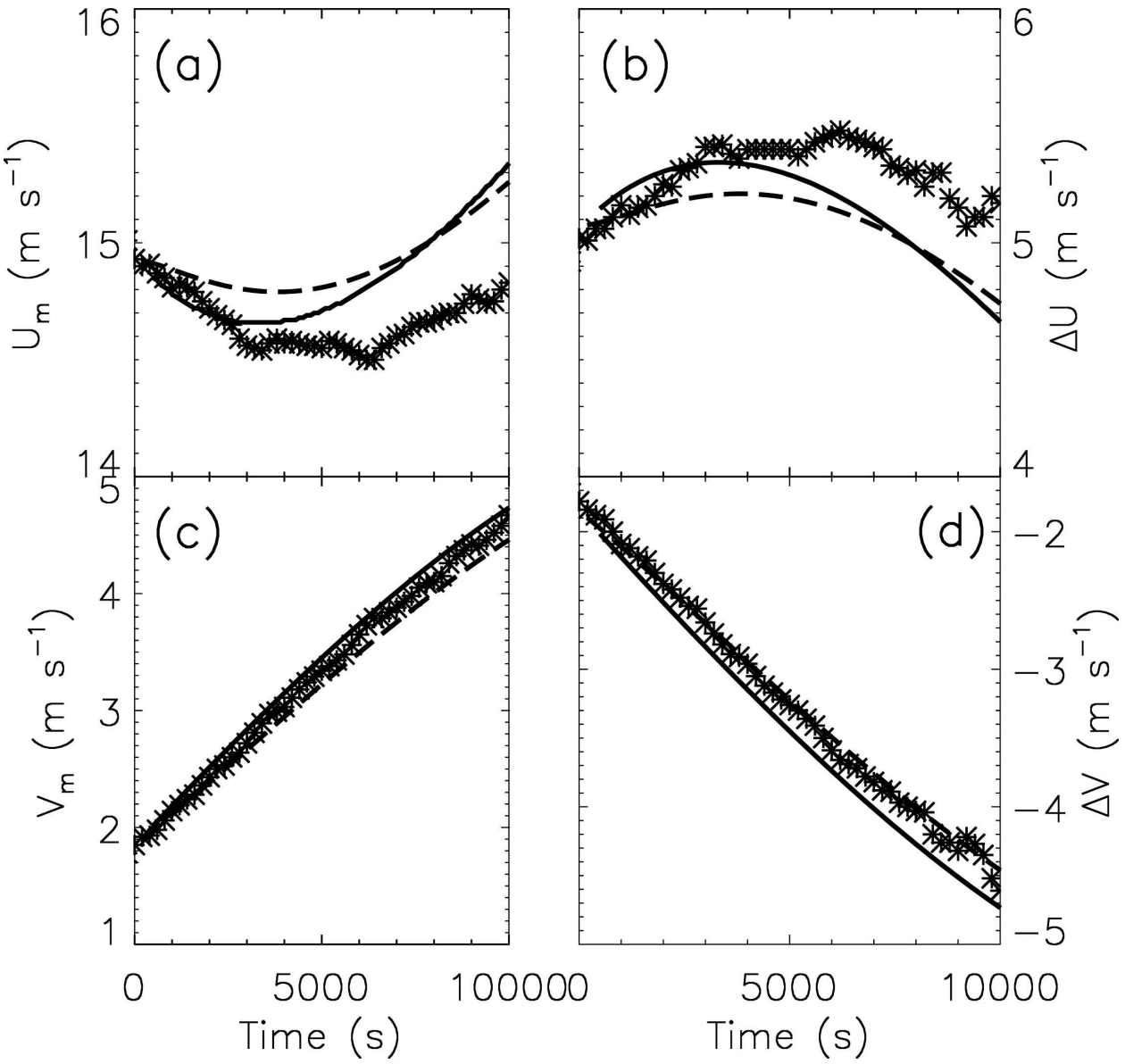

FIG. 9. Same as Fig. 8, but for the strong-inversion case.

budget are analyzed in detail. It was expected that the inclusion of the time tendency of the TKE in β_{ZOJ} would control the contribution of the shear to the entrainment flux at the beginning of the simulation. However, this term, in the cases studied, is only important at the early stages of the boundary layer growth, and it hardly contributes to reducing the value of β_{ZOJ} for $t >$ 3600 s. Consequently, β_{ZOJ} is probably overweighting the contribution of the elevated shear. This is more clearly observed for case S (Fig. 10b), when one expects that the local dissipation effects in the TKE at the inversion are greater when compared with case W (Zeman and Tennekes 1977). In the FOJ, the explicit inclusion of the nonlocal dissipation effects (KIM06) reduces the contribution of the surface shear to the entrainment fluxes by decreasing the value of the constant A_2' that multiplies the surface shear term in β_{FOJ}, relative to the corresponding constant in β_{ZOJ}. Therefore, the FOJ approach produces lower values of β than does ZOJ for a CBL with the same surface wind characteristics.

If the time tendency of the TKE was considered in Eq. (22) then β_{FOJ} decreased, especially at the beginning of the simulations. Therefore, to be able to represent a CBL with different temperature inversion strength and wind shear characteristics, all of the terms

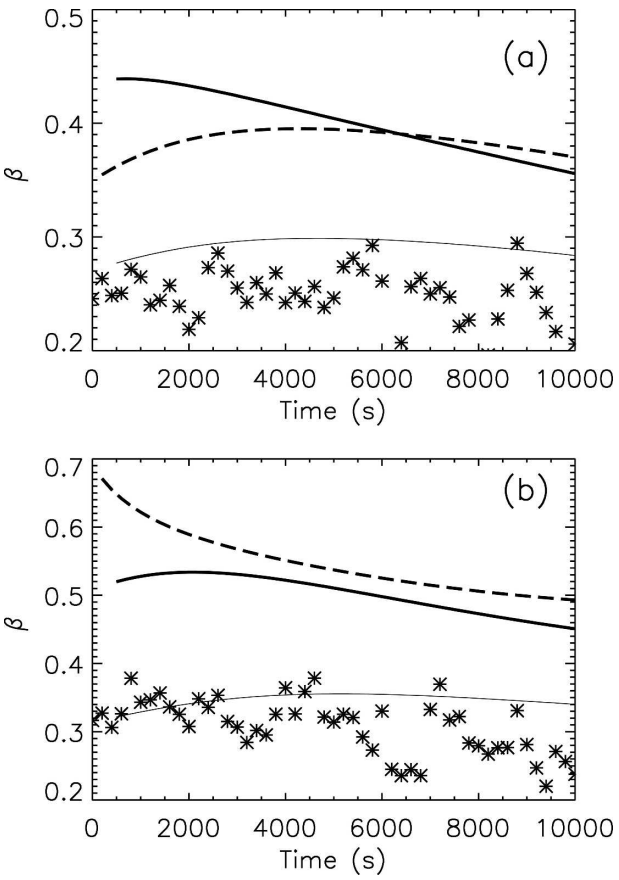

FIG. 10. Time evolution of the ratio between entrainment and surface virtual potential temperature flux β obtained for cases (a) W and (b) S by means of the LES (asterisks), the ZOJ (dashed line), and the FOJ (thick solid line). The thin solid line represents as a reference the time evolution of the entrainment ratio if the original velocity scale at the inversion ($\Delta\hat{U}$) is used.

of the TKE energy equation should be taken into account. In our opinion, this would improve the ability of the MXL to reproduce the LES results.

e. Virtual potential temperature flux partitioning

By observing Fig. 10 one may wrongly conclude that, especially for case S, the MXL does not accurately simulate the amount of heat entrained in the boundary layer. To further study this point, we apply another method to evaluate the calculation of the entrainment heat flux. The flux-partitioning method divides the virtual potential temperature flux into a TKE-consuming part and a TKE-producing part. We compare the ratio between these parts obtained from the LES and the MXL. Three types of heat flux partitioning have been proposed: Eulerian (Lilly 1968; Kraus and Schaller 1978), process (Manins and Turner 1978), and Lagrangian (Stage and Bussinger 1981). However, this last type is difficult to implement directly because each air parcel class with the same vertical velocity and buoyancy should be identified (Randall 1984). See van Zanten et al. (1999) for a comparison between process and Eulerian partitioning applied to several boundary layers. Here, we use the Eulerian partitioning. It is based on the assumption that, at a certain height, the virtual potential temperature flux changes from being a TKE-productive term to being a TKE-consumptive term. The positive part of the total integral of the virtual potential temperature flux P is calculated by integrating the vertical profile of $\overline{w\theta_v}$ over the height range at which it is positive. The negative part N is obtained by integrating $\overline{w\theta_v}$ over the height range at which it is negative. That is, N and P are defined as follows:

$$N = \int_0^{h_2} (\overline{w\theta_v} < 0)\, dz \quad \text{and} \quad P = \int_0^{h_2} (\overline{w\theta_v} > 0)\, dz. \tag{27}$$

In this section, the ratio $A = -NP^{-1}$ is calculated for the MXL and compared with the LES results. In the case of the MXL, as can be observed by looking at Fig. 1, P and N depend on the values of h_1, β, $h_0 = h_1(1 + \beta)^{-1}$, and δ. It is straightforward to show that the ratio reads

$$A = \beta\left[\beta + \frac{\delta}{h_1}(1 + \beta)\right], \tag{28}$$

where β is calculated by means of Eq. (20) for ZOJ ($\delta = 0$), or by using Eq. (22) in the case of FOJ.

Figure 11 shows the time evolution of A obtained by using Eq. (28) for the MXL and integrating the LES virtual potential temperature flux profile during the CBL evolution for the two inversion cases. The large scatter obtained in the LES results is partly due to the fluctuations of h_0, and of h_2 in particular. To explain the differences observed in A between the MXL using both parameterizations, the calculation of P and N is analyzed separately. It is important to note that, because the same surface fluxes are defined for the MXL and the LES, P only depends on the value of h_0 obtained for each model. For the two cases studied, MXL fits well the area of positive virtual potential temperature flux obtained by means of the LES (not shown here). Therefore, the differences between MXL and LES observed in Fig. 11 are only because the MXL is only able to reproduce partially the values of N obtained by means of the LES.

For case W (large δ), the ZOJ underestimates, whereas the FOJ overestimates A obtained by means of the LES. The ZOJ approach, which overestimates β (Fig. 10a), produces lower values of A than the LES

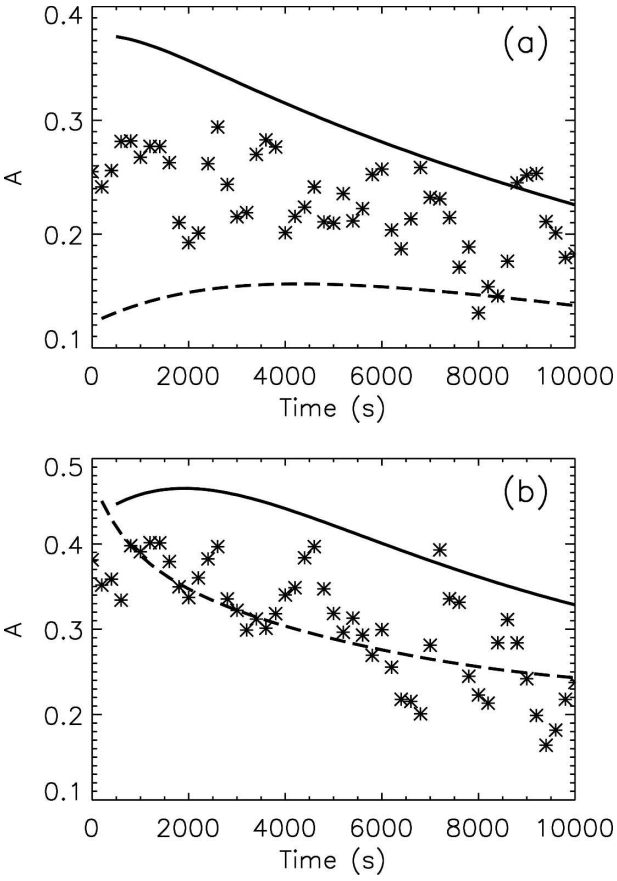

FIG. 11. Time evolution of the ratio between the integral of the negative and positive parts of the virtual potential temperature flux, obtained for cases (a) W and (b) S by means of the LES (asterisks), the ZOJ (dashed line), and the FOJ (solid line).

because of the assumption $\delta = 0$. In this case, this assumption is far from the values obtained by the LES shown in Fig. 5a. In converse, the FOJ approach, which fits the LES δ time evolution (see Fig. 5a) but overestimates the absolute value of the minimum of the virtual potential temperature flux (Fig. 10a), also overestimates A, as was expected.

If case S is analyzed (Fig. 11b), the FOJ overestimates the value of A obtained by means of the LES for same reasons explained above. On the other hand, for this case, the ZOJ fits very well the A obtained by the LES. If a strong inversion strength is considered, δ is lower than for case W. Therefore, for this case, the assumption $\delta = 0$ prescribed in the ZOJ is approximately compensated by the overestimation of the minimum virtual potential temperature flux, and the ZOJ correctly reproduces the value of A obtained by the LES.

From the analysis of the results, we suggest that an intercomparison of different entrainment flux parameterizations with the LES results cannot be only based on the value of the minimum of the virtual potential temperature flux obtained for each parameterization. In our opinion, the use of the Eulerian or process heat flux partitioning is a more suitable method because it takes into account better the regions dominated by the positive heat flux, driven by the surface fluxes and the negative heat flux (entrainment).

f. Statistical analysis

To perform further quantitative analysis of the differences between the LES and the mixed-layer model, the root-mean-square error (rmse) and the root-mean-square vector error (rmsve) were used. These statistical estimators, which have been already used in other atmospheric intercomparison exercises (Cox et al. 1998; Colle et al. 2003), are defined in our study as follows:

$$\mathrm{rmse}_{\mathrm{MXL}} = \left[\frac{\sum_{i=1}^{n} (\Phi_{\mathrm{MXL}}^{i} - \Phi_{\mathrm{LES}}^{i})^2}{n} \right]^{1/2} \quad \text{and} \tag{29}$$

$$\mathrm{rmsve}_{\mathrm{MXL}} = \left\{ \frac{\sum_{i=1}^{n} [(\Psi_{\mathrm{MXL}}^{i} - \Psi_{\mathrm{LES}}^{i})^2 + (\Pi_{\mathrm{MXL}}^{i} - \Pi_{\mathrm{LES}}^{i})^2]}{n} \right\}^{1/2}, \tag{30}$$

where Φ is a scalar variable, in our case h_1, δ, w_e, β, A, Θ_{vm}, or $\Delta\Theta_v$. Also Ψ and Π refer to each wind component, or their respective inversion jumps, n is the total number of times simulated, and subscript MXL refers either to the mixed-layer model using the ZOJ or the FOJ parameterizations. The ZOJ and the LES results are written every 200 s, whereas the FOJ writes its output every 100 s. Between $t = 0$ and $t = 10\,000$ s, the number of incidences of simultaneous output is $n = 48$.

Table 2 shows the rmse or rmsve of the ZOJ and the FOJ for each variable and for cases W and S. For case W, the ZOJ and the FOJ give similar values of the rmse

TABLE 2. Root-mean-square error or root-mean-square vector error of the ZOJ and the FOJ for each of the analyzed variables; M and ΔM represent, respectively, the rmsve of the two components of horizontal wind velocity and their respective inversion jumps.

	W		S	
	ZOJ	FOJ	ZOJ	FOJ
h_1 (m)	23.1	18.5	31.4	14.9
δ (m)	—	106	—	60
β	0.141	0.157	0.238	0.197
A	0.086	0.081	0.047	0.112
w_e (m s^{-1})	0.0033	0.0038	0.006	0.005
Θ_{vm} (K)	0.039	0.061	0.047	0.048
$\Delta\Theta_v$ (K)	0.076	0.373	0.19	0.39
M (m s^{-1})	0.081	0.609	0.31	0.65
ΔM (m s^{-1})	0.16	0.52	0.26	0.58

for most of the considered variables. The high value obtained for δ and $\Delta\Theta_v$ in the case of the FOJ is partially attributed to the scatter of the determination of h_2 from the LES results, especially in case W. Only if the rmsve of the velocities and their inversion jumps are considered can one conclude that the ZOJ simulates the CBL evolution obtained by LES better than the FOJ. The same results are obtained for case S. For this case, though the ZOJ overestimates U_m more than the FOJ, the obtained rmsve, which includes the two components of the horizontal velocity, is slightly lower than the one obtained with the FOJ. A similar result is obtained when one analyzes the inversion jump of the velocities. In summary, Table 2 shows that the ZOJ fits the LES results better.

Figures 12 and 13 summarize the intercomparison of h_1, w_e, β, and A between the MXL and the LES for the weak-inversion and strong-inversion cases, respectively. For case W, Fig. 12 shows how, despite the overestimated values of β and A obtained from the FOJ (ZOJ underestimates A), the LES-calculated boundary layer depth and the entrainment velocity are extremely well fitted by the MXL with both parameterizations of the entrainment flux. For case S (Fig. 13), this pattern is even clearer because the MXL gives values of β that are two times those of the LES but almost perfectly simulates the mixed-layer depth evolution. In this situation, if A is considered, because of the low value of δ obtained by the LES and the overestimation of β by the MXL, the ZOJ approximation produces much better results than the FOJ. From both Table 2 and Figs. 12 and 13, it is clear than the MXL tends to obtain higher values of β when compared with the LES in order to reproduce LES results for the mixed-layer variables and the inversion jumps.

5. Conclusions

Two sheared convective boundary layers with a different temperature stratification in the free atmosphere are studied by means of LES and mixed-layer theory. Different assumptions to describe the depth of the entrainment zone are considered in the MXL: sharp-discontinuity zeroth-order-jump and finite-depth-discontinuity first-order-jump approaches. Furthermore, the entrainment heat flux is represented by using two different parameterizations based on scaling arguments of the TKE budget. We use the LES results to provide the initial values of the MXL and to test the performance of the MXL, with special emphasis on the performance of the entrainment flux parameterizations.

We have shown that the FOJ and ZOJ approaches produce similar results for the two inversion cases. The mixed-layer model results agree well with the boundary layer depth, mixed-layer variables, and inversion jumps obtained from the LES, with a better agreement in the case of weak inversion. If the two MXL approaches are compared, one would expect that as δ increases (weak inversion) the FOJ ($\delta \neq 0$) would better fit the LES data than the ZOJ does. For the cases studied, and considering the mixed-layer variables, this result was not observed.

Regarding the entrainment velocity, both MXL approximately reproduce the LES values with a slight overestimation for the case with a strong inversion. Because of the definitions of the entrainment velocity used in the MXL and the good agreement obtained by the MXL for $\Delta\Theta_v$ and δ, the differences in w_e between MXL and LES are caused because MXL overestimates β obtained by means of LES. One possible explanation for this disagreement is based on the linear profile of the virtual potential temperature flux from the surface up to h_1 assumed by the MXL. This approximation always results in higher values of the entrainment heat flux for the MXL in comparison with the LES results. A second reason is related to the smoothing effect of horizontal averaging, which reduces the value of the entrainment heat flux obtained by LES. Last, the contribution of the shear to the entrainment heat flux could be overstated in the MXL, especially for the ZOJ approach. In the FOJ, the inclusion of the nonlocal dissipation effects explicitly in Eq. (22) reduces the shear contribution to the TKE. This can be more clearly observed in cases with a strong inversion (case S). In addition, under these situations the local dissipation term of the TKE can become important at the entrainment zone. If its contribution was included in the ZOJ and FOJ entrainment parameterizations, the value of the constants η and A_2 of Eqs. (20) and (22), respectively,

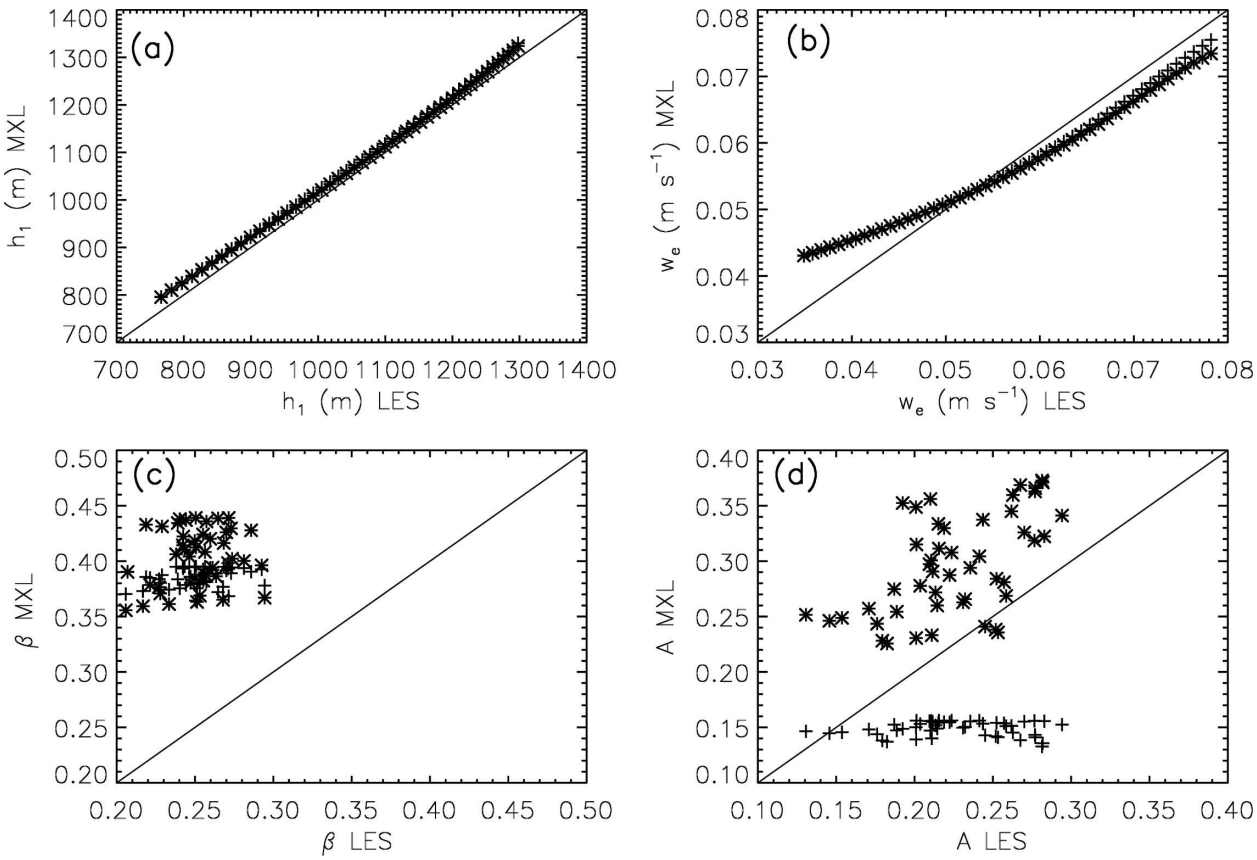

FIG. 12. Scatterplot of the LES vs the ZOJ (crosses) and the FOJ (asterisks) for (a) mixed-layer depth, (b) entrainment velocity, (c) entrainment flux ratio, and (d) virtual potential temperature flux area ratio for the weak-inversion case.

would be reduced. For the FOJ, the time tendency of the TKE could be considered in order to reduce β_{FOJ} at the early stages of the boundary layer development. Therefore, the current study of sheared CBLs by means of the MXL suggests the need to consider all of the terms of the TKE budget to parameterize the MXL entrainment heat flux.

The entrainment heat flux parameterizations included in the MXL have also been studied by using Eulerian heat flux partitioning. If the ratio between positive and negative areas of the virtual potential temperature flux A are considered, the LES and MXL results agree more closely than they do if the ratio of the entrainment flux to the surface flux is used as the basis for comparison, especially for the ZOJ. In our opinion, the comparison only using the single values of the virtual potential temperature flux could lead to misleading results. The heat flux partitioning method is more appropriate because it accounts for the distribution of the heat in the whole boundary layer. For this reason, we suggest that in any entrainment parameterization intercomparison, in addition to the comparison of β itself, the comparison of the heat flux partitioning has to be considered in order to analyze the performance of each parameterization.

In summary, in this work we show that the MXL can accurately reproduce the evolution of a realistic sheared CBL. The parameterizations of the entrainment heat flux included in the MXL take into account the main mechanisms that control the turbulent kinetic energy budget. These parameterizations consequently provide values of β that vary during the day and that, depending on the CBL characteristics, can be larger than 0.2. Furthermore, we show that the most simple mixed-layer approach, the ZOJ, gives results similar to those of the FOJ. However, the two entrainment parameterizations included in the MXL do not consider the local effects of some of the TKE terms in the inversion zone, such as the dissipation or the shear. These local effects lead one to consider, in the scaling of the dissipation and shear terms, a characteristic length scale different from h_1—for instance, the depth of the inversion layer.

The agreement obtained for the boundary layer

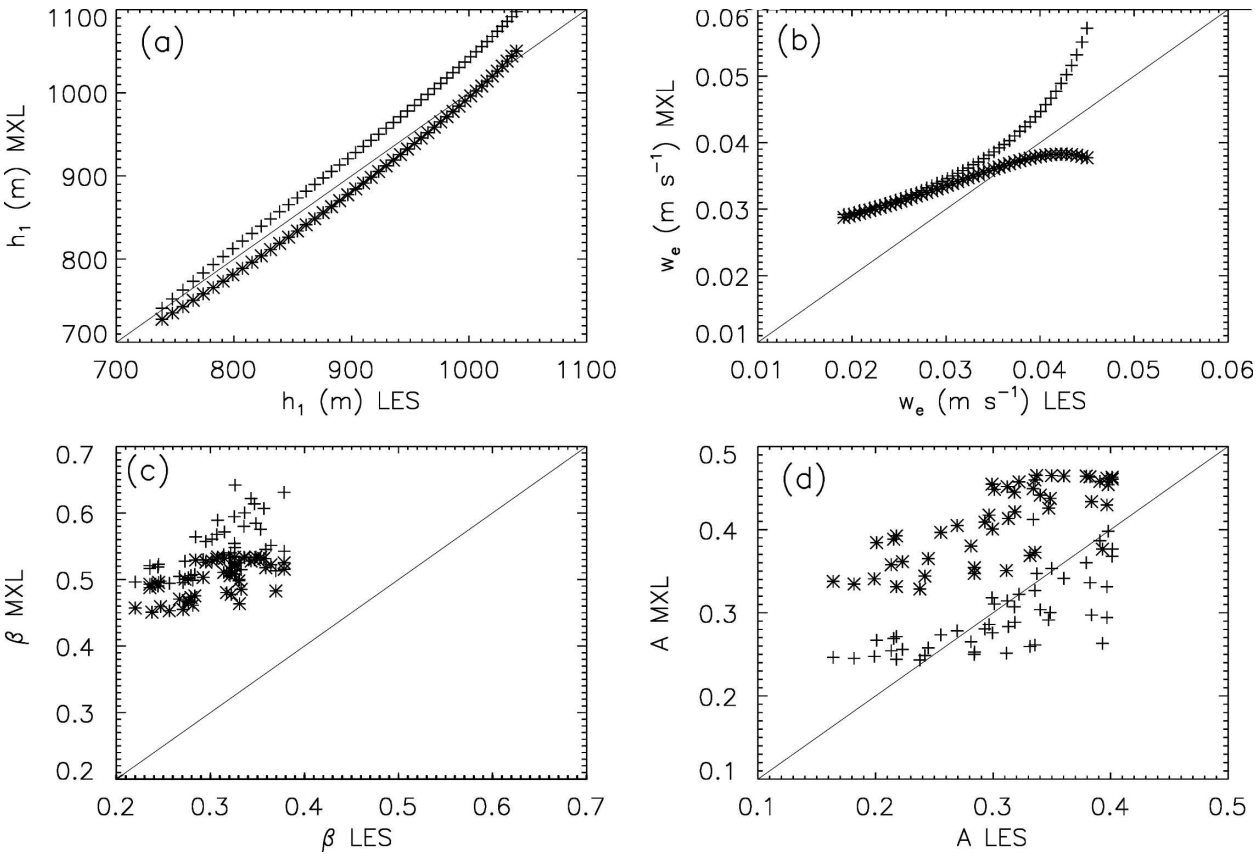

FIG. 13. Same as Fig. 12, but for the strong-inversion case.

depth (h_1) and mixed-layer variables (Θ_{vm}, U_m, and V_m) is particularly encouraging, because these variables are fundamental for describing the diurnal variability of the boundary layer in general circulation and chemical transport models. The results shows that both parameterizations of the entrainment flux (the ZOJ and the FOJ) provide an accurate description of it as a function of the relevant processes that drive this flux at the interface between the boundary layer and the free troposphere.

Acknowledgments. This work was supported by the visiting study program of the Korea Science and Engineering Foundations (KOSEF), the NCAR visiting scientist program, the Stichting Nationale Computerfaciliteiten [National Computing Facilities Foundation (NCF)] with Project SG-132 for the use of supercomputing facilities, with financial support from the Netherlandse Organisatie voor Wetenschappelijk Onderzoek [Netherlands Organization for Scientific Research (NWO)] and Spanish MCYT Scientific Project REN2003-03436. Author J. Vilà was partially supported during his visit to NCAR by the NWO Project R76-241. We acknowledge the critical remarks and suggestions given by the three reviewers, which helped us to greatly improve the manuscript.

REFERENCES

Angevine, W. M., A. W. Grimsdell, A. McKeen, and J. M. Warnock, 1998: Entrainment results from the Flatland boundary layer experiments. *J. Geophys. Res.,* **103,** 13 689–13 701.

Artaz, M. A., and J. C. André, 1980: Similarity studies of entrainment in convective mixed layers. *Bound.-Layer Meteor.,* **19,** 51–66.

Betts, A. K., 1973: Non-precipitating cumulus convection and its parameterization. *Quart. J. Roy. Meteor. Soc.,* **99,** 178–196.

——, 1974: Reply to comment on the paper "Non-precipitating cumulus convection and its parameterization." *Quart. J. Roy. Meteor. Soc.,* **100,** 469–471.

——, R. L. Desjardins, and J. I. MacPherson, 1992: Budget analysis of the boundary layer grid flights during FIFE 1987. *J. Geophys. Res.,* **97,** 18 533–18 546.

Boers, R., E. W. Eloranta, and R. L. Coulter, 1984: Lidar parameterizations of mixed layer dynamics: Tests of parameterized entrainment models of mixed layer growth rate. *J. Climate Appl. Meteor.,* **23,** 247–266.

Carson, D. J., 1973: The development of a dry inversion-capped convectively unstable boundary layer. *Quart. J. Roy. Meteor. Soc.,* **99,** 450–467.

Cattle, H., and K. J. Weston, 1975: Budget studies of heat flux

profiles in the convective boundary layer over land. *Quart. J. Roy. Meteor. Soc.,* **101,** 353–363.

Caughey, S. J., and S. G. Palmer, 1979: Some aspects of turbulence structure through the depth of the convective boundary layer. *Quart. J. Roy. Meteor. Soc.,* **105,** 801–827.

Colle, B. A., J. B. Olson, and J. S. Tongue, 2003: Multiseason verification of the MM5. Part I: Comparison with the Eta Model over the central and eastern United States and impact of MM5 resolution. *Wea. Forecasting,* **18,** 431–457.

Conzemius, R., and E. Fedorovich, 2004: Numerical models of entrainment into sheared convective boundary layers evaluated through large eddy simulations. Preprints, *16th Symp. on Boundary Layer and Turbulence,* Portland, ME, Amer. Meteor. Soc., CD-ROM, 5.6.

Cox, R., B. L. Bauer, and T. Smith, 1998: A mesoscale model intercomparison. *Bull. Amer. Meteor. Soc.,* **79,** 265–283.

Cuijpers, J. W. M., and P. G. Duynkerke, 1993: Large eddy simulation of trade wind cumulus clouds. *J. Atmos. Sci.,* **50,** 3894–3908.

——, and A. A. M. Holtslag, 1998: Impact of skewness and nonlocal effect on scalar and buoyancy fluxes in convective boundary layers. *J. Atmos. Sci.,* **55,** 151–162.

Culf, A. D., 1992: An application of simple models to Sahelian convective boundary-layer growth. *Bound.-Layer Meteor.,* **58,** 1–18.

Deardorff, J. W., G. E. Willis, and B. H. Stockton, 1980: Laboratory studies of the entrainment zone of a convectively mixed layer. *J. Fluid Mech.,* **100,** 41–64.

de Arellano, J. V.-G., B. Gioli, F. Miglietta, H. J. J. Jonker, H. K. Baltink, R. W. A. Hutjes, and A. A. M. Holtslag, 2004: Entrainment process of carbon dioxide in the atmospheric boundary layer. *J. Geophys. Res.,* **109,** D18110, doi:10.1029/2004JD004725.

Driedonks, A. G. M., 1981: Dynamics of the well-mixed atmospheric boundary layer. Ph.D. dissertation, Vrije Universiteit te Amsterdam, 189 pp.

——, 1982: Models and observations of the growth of the atmospheric boundary layer. *Bound.-Layer Meteor.,* **23,** 283–306.

——, and H. Tennekes, 1984: Entrainment effects in the well-mixed atmospheric boundary layer. *Bound.-Layer Meteor.,* **30,** 75–105.

Dubosclard, G., 1980: A comparison between observed values and predicted values for the entrainment coefficient in the planetary boundary layer. *Bound.-Layer Meteor.,* **18,** 473–483.

Fairall, C. W., 1984: Wind shear enhancement of entrainment and refractive index structure parameter at the top of a turbulent mixed layer. *J. Atmos. Sci.,* **41,** 3472–3484.

Fedorovich, E., 1995: Modeling the atmospheric convective boundary layer within a zero-order jump approach: An extended theoretical framework. *J. Appl. Meteor.,* **34,** 1916–1928.

——, F. T. M. Nieuwstadt, and R. Kaiser, 2001: Numerical and laboratory study of a horizontally evolving convective boundary layer. Part II: Effects of elevated wind shear and surface roughness. *J. Atmos. Sci.,* **58,** 546–560.

——, R. Conzemius, and D. Mironov, 2004a: Convective entrainment into a shear-free, linearly stratified atmosphere: Bulk models reevaluated through large eddy simulations. *J. Atmos. Sci.,* **61,** 281–295.

——, and Coauthors, 2004b: Entrainment into sheared convective boundary layers as predicted by different large eddy simulation codes. Preprints, *16th Symp. on Boundary Layers and Turbulence,* Portland, ME, Amer. Meteor. Soc., CD-ROM, P4.7.

Flamant, C., and J. Pelon, 1996: Atmospheric boundary-layer structure over the Mediterranean during a Tramontane event. *Quart. J. Roy. Meteor. Soc.,* **122,** 1741–1778.

——, ——, P. H. Flamant, and P. Durand, 1997: Lidar determination of the entrainment zone thickness at the top of the unstable marine atmospheric boundary layer. *Bound.-Layer Meteor.,* **83,** 247–284.

——, ——, B. Brashers, and R. A. Brown, 1999: Evidence of a mixed-layer dynamics contribution to the entrainment process. *Bound.-Layer Meteor.,* **93,** 47–73.

Garratt, J. R., 1992: *The Atmospheric Boundary Layer*. Cambridge University Press, 316 pp.

——, J. C. Wyngaard, and R. J. Francey, 1982: Winds in the atmospheric boundary layer—Prediction and observation. *J. Atmos. Sci.,* **39,** 1307–1316.

Gryning, S. E., and E. Batchvarova, 1990: Analytical model for the growth of the coastal internal boundary layer during onshore flow. *Quart. J. Roy. Meteor. Soc.,* **116,** 187–203.

——, and ——, 1994: Parameterization of the depth of the entrainment zone above the daytime mixed layer. *Quart. J. Roy. Meteor. Soc.,* **120,** 47–58.

Källstrand, B., and A.-S. Smedman, 1997: A case study of the near-neutral coastal internal boundary-layer growth: Aircraft measurements compared with different model estimates. *Bound.-Layer Meteor.,* **85,** 1–33.

Kim, S.-W., S.-U. Park, and C.-H. Moeng, 2003: Entrainment processes in the convective boundary layer with varying wind shear. *Bound.-Layer Meteor.,* **108,** 221–245.

——, ——, D. Pino, and J. Vilà-Guerau de Arellano, 2006: Entrainment parameterization in a sheared convective boundary layer by using a first-order jump model. *Bound.-Layer Meteor.,* in press.

Kraus, H., and E. Schaller, 1978: A note on the closure in Lilly-type inversion models. *Tellus,* **30,** 284–288.

Lilly, D. K., 1968: Models of cloud-topped mixed layer under a strong inversion. *Quart. J. Roy. Meteor. Soc.,* **94,** 292–309.

——, 2002a: Entrainment into mixed layers. Part I: Sharp-edged and smoothed tops. *J. Atmos. Sci.,* **59,** 3340–3352.

——, 2002b: Entrainment into mixed layers. Part II: A new closure. *J. Atmos. Sci.,* **59,** 3353–3361.

Lock, A. P., and M. K. MacVean, 1999: The parametrization of entrainment driven by surface heating and cloud-top cooling. *Quart. J. Roy. Meteor. Soc.,* **125,** 271–299.

Mahrt, L., and D. H. Lenschow, 1976: Growth dynamics of the convectively mixed layer. *J. Atmos. Sci.,* **33,** 41–51.

Manins, P. C., and J. S. Turner, 1978: The relation between flux ratio and the energy ratio in convectively mixed layers. *Quart. J. Roy. Meteor. Soc.,* **104,** 39–44.

Moeng, C.-H., and P. P. Sullivan, 1994: A comparison of shear- and buoyancy-driven planetary boundary layer flows. *J. Atmos. Sci.,* **51,** 999–1022.

Pelly, J. L., and S. E. Belcher, 2001: A mixed-layer model of the well-mixed stratocumulus-topped boundary layer. *Bound.-Layer Meteor.,* **100,** 171–187.

Pino, D., J. Vilà-Guerau de Arellano, and P. G. Duynkerke, 2003: The contribution of shear to the evolution of a convective boundary layer. *J. Atmos. Sci.,* **60,** 1913–1926.

Randall, D. A., 1984: Buoyant production and consumption of turbulent kinetic energy in cloud-topped mixed layers. *J. Atmos. Sci.,* **41,** 402–413.

Rayment, R., and C. J. Readings, 1974: Case study of the structure

and energetics of an inversion. *Quart. J. Roy. Meteor. Soc.,* **100,** 221–233.

Sorbjan, Z., 2004: Large-eddy simulations of the baroclinic mixed layer. *Bound.-Layer Meteor.,* **112,** 57–80.

Stage, S., and J. Bussinger, 1981: A model for entrainment into a cloud-topped marine boundary layer. Part II: Discussion of model behavior and comparison with other models. *J. Atmos. Sci.,* **38,** 2230–2242.

Stull, R. B., 1976a: The energetics of entrainment across a density interface. *J. Atmos. Sci.,* **33,** 1260–1267.

——, 1976b: Mixed-layer depth model based on turbulent energetics. *J. Atmos. Sci.,* **33,** 1268–1278.

——, 1988: *An Introduction to Boundary Layer Meteorology*. Kluwer Academic, 670 pp.

Sullivan, P. P., C.-H. Moeng, B. Stevens, D. H. Lenschow, and S. D. Mayor, 1998: Structure of the entrainment zone capping the convective atmospheric boundary layer. *J. Atmos. Sci.,* **55,** 3042–3064.

Tennekes, H., 1973: A model for the dynamics of the inversion above a convective boundary layer. *J. Atmos. Sci.,* **30,** 558–567.

——, and A. G. M. Driedonks, 1981: Basic entrainment equations for the atmospheric boundary layer. *Bound.-Layer Meteor.,* **20,** 515–531.

van Zanten, M. C., P. G. Duynkerke, and J. W. M. Cuijpers, 1999: Entrainment parameterization in convective boundary layers. *J. Atmos. Sci.,* **56,** 813–828.

Villani, M. G., A. Maurizi, and F. Tampieri, 2005: Discussion and applications of slab models of the convective boundary layer based on turbulent kinetic energy budget parameterizations. *Bound.-Layer Meteor.,* **114,** 539–556.

Vinuesa, J.-F., and J. Vilà-Guerau de Arellano, 2005: Introducing effective reaction rates to account for the inefficient mixing of the convective boundary layer. *Atmos. Environ.,* **39,** 445–461.

Zeman, O., and H. Tennekes, 1977: Parameterization of the turbulent energy budget at the top of the daytime atmospheric boundary layer. *J. Atmos. Sci.,* **34,** 111–123.

Zilitinkevich, S. S., 1975: Comments on "A model for the dynamics of the inversion above a convective boundary layer." *J. Atmos. Sci.,* **32,** 991–992.

——, 1991: *Turbulent Penetrative Convection.* Avebury Technical, 180 pp.